Since January 2020 Elsevier has created a COVID-19 resource centre with free information in English and Mandarin on the novel coronavirus COVID-19. The COVID-19 resource centre is hosted on Elsevier Connect, the company's public news and information website.

Clinical and Translational Report

Cell Host & Microbe

Replication-Competent Vesicular Stomatitis Virus Vaccine Vector Protects against SARS-CoV-2-Mediated Pathogenesis in Mice

Graphical Abstract

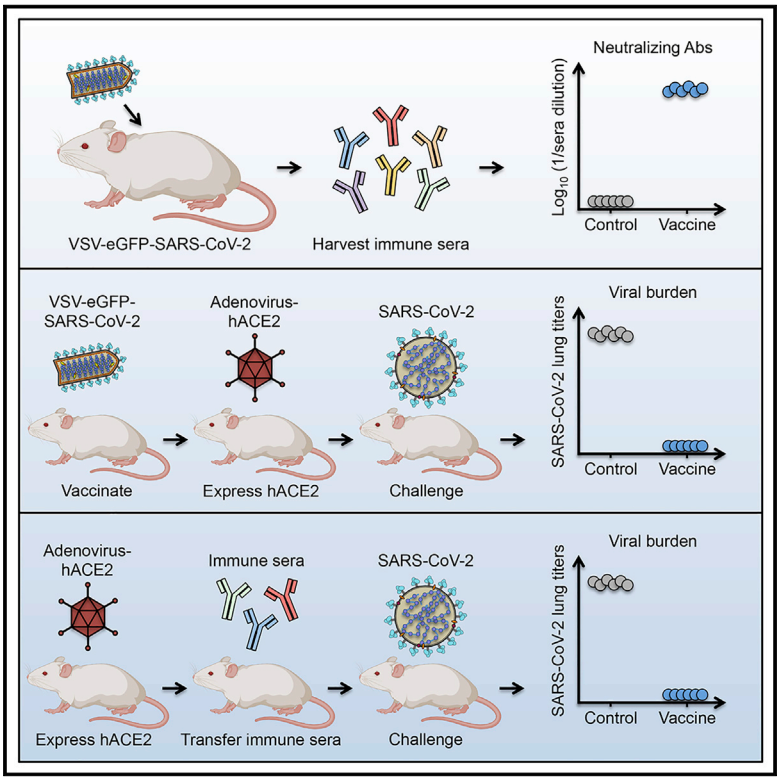

Highlights

- A replicating VSV-SARS-CoV-2 vaccine induces high-titer neutralizing antibodies
- Infectious SARS-CoV-2 is undetectable in the lung of vaccinated mice post-challenge
- SARS-CoV-2-induced lung inflammation and pathology is decreased in vaccinated mice
- Transfer of vaccine-derived immune sera to naive mice protects against SARS-CoV-2

Authors

James Brett Case, Paul W. Rothlauf, Rita E. Chen, ..., Daved H. Fremont, Sean P.J. Whelan, Michael S. Diamond

Correspondence

spjwhelan@wustl.edu (S.P.J.W.), diamond@wusm.wustl.edu (M.S.D.)

In Brief

Case, Rothlauf et al. report the efficacy of a replicating VSV-based SARS-CoV-2 vaccine. Immunized hACE2-expressing mice challenged with SARS-CoV-2 are protected against lung infection, inflammation, and pneumonia. Neutralizing antibodies are a correlate of this protection, as passive transfer of vaccine-derived immune sera protects naive mice from subsequent SARS-CoV-2 challenge.

Case et al., 2020, Cell Host & Microbe *28*, 465–474
September 9, 2020
https://doi.org/10.1016/j.chom.2020.07.018

CellPress

Cell Host & Microbe

CellPress

Clinical and Translational Report

Replication-Competent Vesicular Stomatitis Virus Vaccine Vector Protects against SARS-CoV-2-Mediated Pathogenesis in Mice

James Brett Case,[1,8] Paul W. Rothlauf,[2,7,8] Rita E. Chen,[1,3] Natasha M. Kafai,[1,3] Julie M. Fox,[1] Brittany K. Smith,[3] Swathi Shrihari,[1] Broc T. McCune,[1] Ian B. Harvey,[3] Shamus P. Keeler,[1,6] Louis-Marie Bloyet,[2] Haiyan Zhao,[3] Meisheng Ma,[3] Lucas J. Adams,[3] Emma S. Winkler,[1,3] Michael J. Holtzman,[1,6] Daved H. Fremont,[2,3,4,5] Sean P.J. Whelan,[2,*] and Michael S. Diamond[1,2,3,5,9,*]

[1]Department of Medicine, Washington University School of Medicine, St. Louis, MO, USA
[2]Department of Molecular Microbiology, Washington University School of Medicine, St. Louis, MO, USA
[3]Department of Pathology & Immunology, Washington University School of Medicine, St. Louis, MO, USA
[4]Biochemistry & Molecular Biophysics, Washington University School of Medicine, St. Louis, MO, USA
[5]The Andrew M. and Jane M. Bursky Center for Human Immunology & Immunotherapy Programs, Washington University School of Medicine, St. Louis, MO, USA
[6]Division of Pulmonary and Critical Care Medicine, Washington University School of Medicine, St. Louis, MO, USA
[7]Program in Virology, Harvard Medical School, Boston, MA, USA
[8]These authors contributed equally
[9]Lead Contact
*Correspondence: spjwhelan@wustl.edu (S.P.J.W.), diamond@wusm.wustl.edu (M.S.D.)
https://doi.org/10.1016/j.chom.2020.07.018

SUMMARY

Severe acute respiratory syndrome coronavirus 2 (SARS-CoV-2) has caused millions of human infections, and an effective vaccine is critical to mitigate coronavirus-induced disease 2019 (COVID-19). Previously, we developed a replication-competent vesicular stomatitis virus (VSV) expressing a modified form of the SARS-CoV-2 spike gene in place of the native glycoprotein gene (VSV-eGFP-SARS-CoV-2). Here, we show that vaccination with VSV-eGFP-SARS-CoV-2 generates neutralizing immune responses and protects mice from SARS-CoV-2. Immunization of mice with VSV-eGFP-SARS-CoV-2 elicits high antibody titers that neutralize SARS-CoV-2 and target the receptor binding domain that engages human angiotensin-converting enzyme-2 (ACE2). Upon challenge with a human isolate of SARS-CoV-2, mice that expressed human ACE2 and were immunized with VSV-eGFP-SARS-CoV-2 show profoundly reduced viral infection and inflammation in the lung, indicating protection against pneumonia. Passive transfer of sera from VSV-eGFP-SARS-CoV-2-immunized animals also protects naive mice from SARS-CoV-2 challenge. These data support development of VSV-SARS-CoV-2 as an attenuated, replication-competent vaccine against SARS-CoV-2.

INTRODUCTION

Severe acute respiratory syndrome coronavirus 2 (SARS-CoV-2), a positive-sense, single-stranded, enveloped RNA virus, is the causative agent of coronavirus disease 2019 (COVID-19). Since its outbreak in Wuhan, China in December 2019, SARS-CoV-2 has infected millions of individuals and caused hundreds of thousands of deaths worldwide. Because of its capacity for human-to-human transmission, including from asymptomatic individuals, SARS-CoV-2 has caused a pandemic, leading to significant political, economic, and social disruption (Bai et al., 2020). Currently, social quarantine, physical distancing, and vigilant hand hygiene are the only effective preventative measures against SARS-CoV-2 infections. Thus, effective countermeasures, particularly vaccines, are urgently needed to curtail the virus spread, limit morbidity and mortality, and end the COVID-19 pandemic.

The SARS-CoV-2 spike (S) protein mediates the receptor-binding and membrane fusion steps of viral entry. The S protein also is the primary target of neutralizing antibodies (Baum et al., 2020; Chi et al., 2020; Pinto et al., 2020; Rogers et al., 2020) and can elicit $CD4^+$ and $CD8^+$ T cell responses (Grifoni et al., 2020). Several SARS-CoV-2 vaccine platforms based on the S protein are being developed, including adenovirus-based vectors, inactivated virus formulations, recombinant subunit vaccines, and DNA- and mRNA-based strategies (Amanat and Krammer, 2020; Lurie et al., 2020). Although several of these vaccines have entered human clinical trials, efficacy data in animals has been published for only a subset of these candidates (Gao et al., 2020; Yu et al., 2020).

We recently reported the generation and characterization of a replication-competent, VSV (designated VSV-eGFP-SARS-CoV-2) that expresses a modified form of the SARS-CoV-2 S protein (Case et al., 2020). We demonstrated that monoclonal antibodies, human sera, and soluble ACE2-Fc potently inhibit VSV-eGFP-SARS-CoV-2 infection in a manner nearly identical to a clinical isolate of SARS-CoV-2. This suggests that chimeric VSV displays the S protein in an antigenic form that resembles native infectious SARS-CoV-2. Because of this data, we hypothesized that a replicating VSV-eGFP-SARS-CoV-2 might serve as an alternative platform for vaccine development. Indeed, an analogous replication-competent recombinant VSV vaccine expressing the Ebola virus (EBOV) glycoprotein protects against lethal EBOV challenge in several animal models (Garbutt et al., 2004; Jones et al., 2005), is safe in immunocompromised nonhuman primates (Geisbert et al., 2008), and was approved for clinical use in humans after successful clinical trials (Henao-Restrepo et al., 2017; Henao-Restrepo et al., 2015). Other live-attenuated recombinant VSV-based vaccines are in pre-clinical development for HIV-1, hantaviruses, filoviruses, arenaviruses, and influenza viruses (Brown et al., 2011; Furuyama et al., 2020; Garbutt et al., 2004; Geisbert et al., 2005; Jones et al., 2005).

Here, we determined the immunogenicity and *in vivo* efficacy of VSV-eGFP-SARS-CoV-2 as a vaccine in a mouse model of SARS-CoV-2 pathogenesis. We demonstrate that a single dose of VSV-eGFP-SARS-CoV-2 generates a robust neutralizing antibody response that targets both the SARS-CoV-2 S protein and the receptor binding domain (RBD) subunit. Upon challenge with infectious SARS-CoV-2, mice immunized with one or two doses of VSV-eGFP-SARS-CoV-2 showed significant decreases in lung and peripheral organ viral loads, pro-inflammatory cytokine responses, and consequent lung disease. VSV-eGFP-SARS-CoV-2-mediated protection likely is due in part to antibodies, because passive transfer of immune sera to naive mice limits infection after SARS-CoV-2 challenge. This study paves the way for further development of a VSV-vectored SARS CoV-2 vaccine.

RESULTS

Generation of a VSV-eGFP-SARS-CoV-2 as a Vaccine Platform

We previously reported a chimeric, replication-competent VSV expressing the SARS-CoV-2 S protein as an effective platform for measuring neutralizing antibodies (Case et al., 2020). Because replication-competent VSVs are in clinical use as vaccines for emerging RNA viruses or in pre-clinical development (Fathi et al., 2019), we tested whether VSV-eGFP-SARS-CoV-2 could protect mice against SARS-CoV-2.

To examine the immune response to VSV-eGFP-SARS-CoV-2, we immunized four-week-old BALB/c mice with 10^6 plaque-forming units (PFU) of VSV-eGFP-SARS-CoV-2 or a control VSV-eGFP (Figure 1A). As murine ACE2 does not serve as a receptor for SARS-CoV-2, we spiked our preparation of VSV-eGFP-SARS-CoV-2 with trace amounts of VSV G to permit a single round of infection, an approach used previously for SARS-CoV (Kapadia et al., 2008) (Figure S1). At 28 days post-priming, one cohort of animals was boosted with the homologous vaccine. Serum was isolated from all animals at three weeks post-priming or boosting, and IgG titers against recombinant SARS-CoV-2 S protein or the RBD were determined by ELISA (Figures 1B and 1C). Immunization with VSV-eGFP-SARS-CoV-2 induced high levels of anti-S and anti-RBD-specific IgG compared to control VSV-eGFP with reciprocal median serum endpoint titers of 3.2×10^5 and 2.7×10^6 (anti-S) and 1.1×10^4 and 1.4×10^5 (anti-RBD) for one and two doses of vaccine, respectively.

We measured neutralizing antibody titers against SARS-CoV-2 after priming or boosting by using a focus-reduction neutralization test (Case et al., 2020). Immunization with a single- or two-dose regimen of VSV-eGFP-SARS-CoV-2 induced neutralizing antibodies (median titers of 1/59 and 1/5,206, respectively) whereas the control VSV-eGFP vaccine did not (Figure 1D). Boosting was effective and resulted in a 90-fold increase in neutralizing activity after the second dose of VSV-eGFP-SARS-CoV-2. Collectively, these data suggest that VSV-eGFP-SARS-CoV-2 is immunogenic and elicits high titers of antibodies that neutralize infection and target the RBD of the SARS-CoV-2 S protein.

Because VSV-eGFP-SARS-CoV-2 might not enter efficiently into cells of conventional BALB/c mice lacking the human ACE2 (hACE2) receptor, we confirmed immunogenicity in K18-hACE2 transgenic C57BL/6 mice, in which hACE2 expression is driven by an epithelial cell promoter (McCray et al., 2007). We immunized four-week-old K18-hACE2 transgenic mice by intranasal route with 10^6 PFU of VSV-eGFP-SARS-CoV-2 or VSV-eGFP control. Serum was isolated at three weeks post-priming, and IgG titers against recombinant SARS-CoV-2 RBD were measured by ELISA. We detected robust IgG responses against RBD in VSV-eGFP-SARS-CoV-2 but not VSV-eGFP vaccinated mice (Figure 1E). Immunoglobulin subclass analysis indicated substantial class-switching occurred, because high levels of IgG2b and IgG2c against RBD were detected (Figure 1E). Finally, we detected neutralizing antibodies against SARS-CoV-2 (median titer of 1/325) three weeks after immunizing K18-hACE2 transgenic mice with a single dose of VSV-eGFP-SARS-CoV-2 but not VSV-eGFP (Figure 1F).

VSV-eGFP-SARS-CoV-2 Protects Mice against SARS-CoV-2 Infection

Four weeks after priming or priming and boosting, BALB/c mice were administered 2 mg of anti-Ifnar1 mAb; although not required for infection, this treatment augments pathogenesis of SARS-CoV-2 in the lung and creates a stringent disease model for vaccine protection (Hassan et al., 2020). The following day, mice were inoculated via the intranasal route with a replication-defective adenovirus expressing human ACE2 (AdV-hACE2) that enables receptor expression in the lungs (Hassan et al., 2020). Five days later, mice were challenged via the intranasal route with 3×10^5 PFU of SARS-CoV-2 (strain 2019 n-CoV/USA_WA1/2020) to evaluate vaccine protection (Figure 1A). We subsequently measured viral yield both by plaque forming and RT-qPCR assays. At day four post-infection (dpi) infectious virus was not recovered from lungs of mice vaccinated either with one or two doses of VSV-eGFP-SARS-CoV-2 (Figure 2A). For mice receiving only one dose of VSV-eGFP-SARS-CoV-2 vaccine, we observed a trend toward decreased levels of viral RNA in the lung, spleen, and heart at 4 dpi and in the lung and spleen

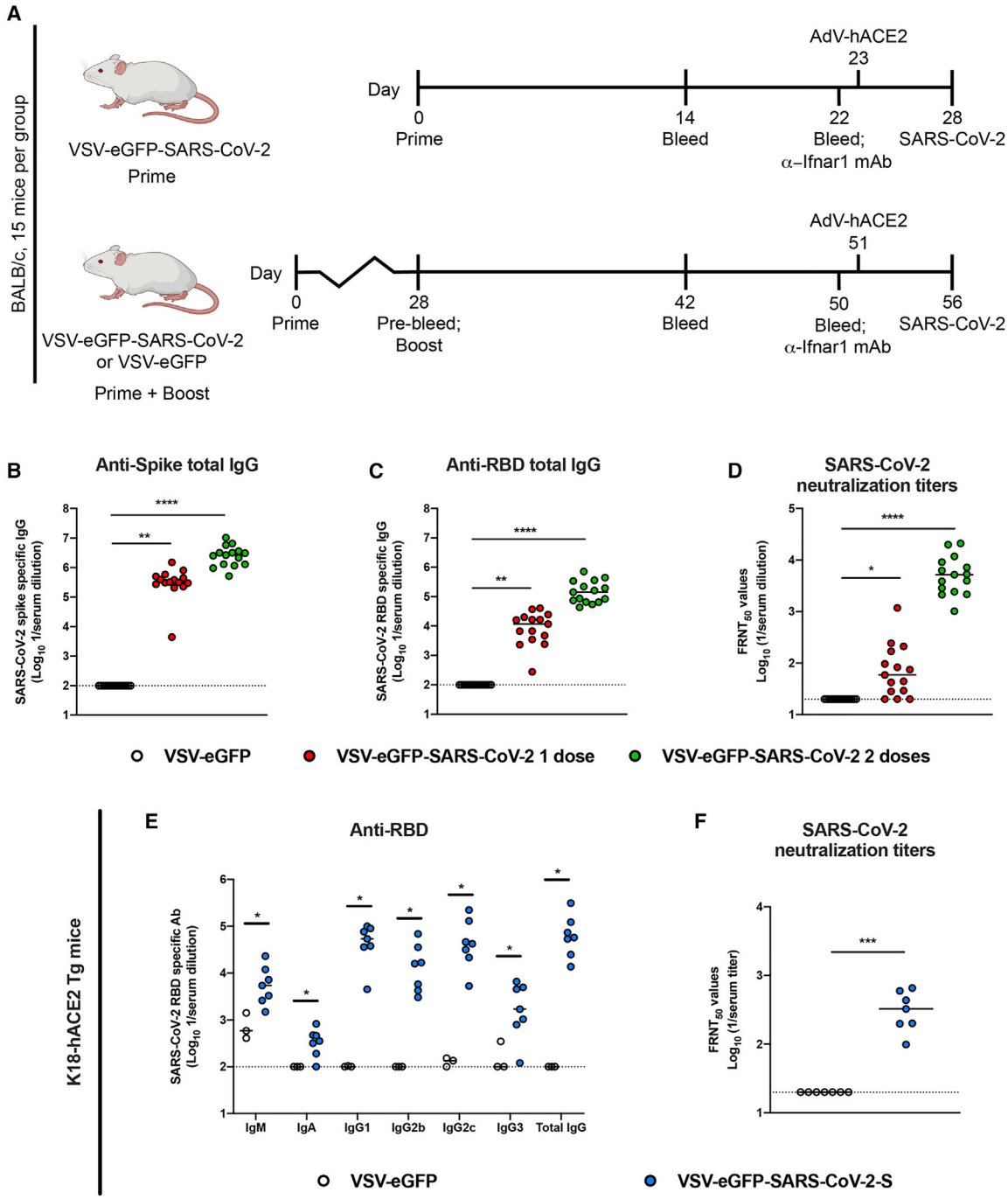

Figure 1. Immunogenicity of VSV-eGFP-SARS-CoV-2

(A) Scheme of vaccination and SARS-CoV-2 challenge.

(B–D) Four-week-old female BALB/c mice were immunized with VSV-eGFP or VSV-eGFP-SARS-CoV-2. Some of the immunized mice were boosted with their respective vaccines four weeks after primary vaccination. IgG responses in the sera of vaccinated mice were evaluated three weeks after priming or boosting by ELISA for binding to SARS-CoV-2 S (B) or RBD (C) or two weeks after priming or boosting by focus reduction neutralization test (FRNT) (D) (n = 15 per group; one-way ANOVA with Dunnett's post-test: ****$p < 0.0001$). Bars indicate median values.

(E and F) Four-week-old K18-hACE2 transgenic mice were immunized with VSV-eGFP or VSV-eGFP-SARS-CoV-2 via an intranasal route. Three weeks later, serum was harvested and levels of anti-SARS-CoV-2 RBD antibodies (IgM, IgA, IgG1, IgG2b, IgG2c, IgG3, and total IgG) were determined by ELISA (n = 3–7 per group; Mann-Whitney test: *$p < 0.05$) (E), or neutralizing antibody titers were determined by FRNT (F) (n = 7 per group; Mann-Whitney test: ***$p < 0.001$).

See Figure S1.

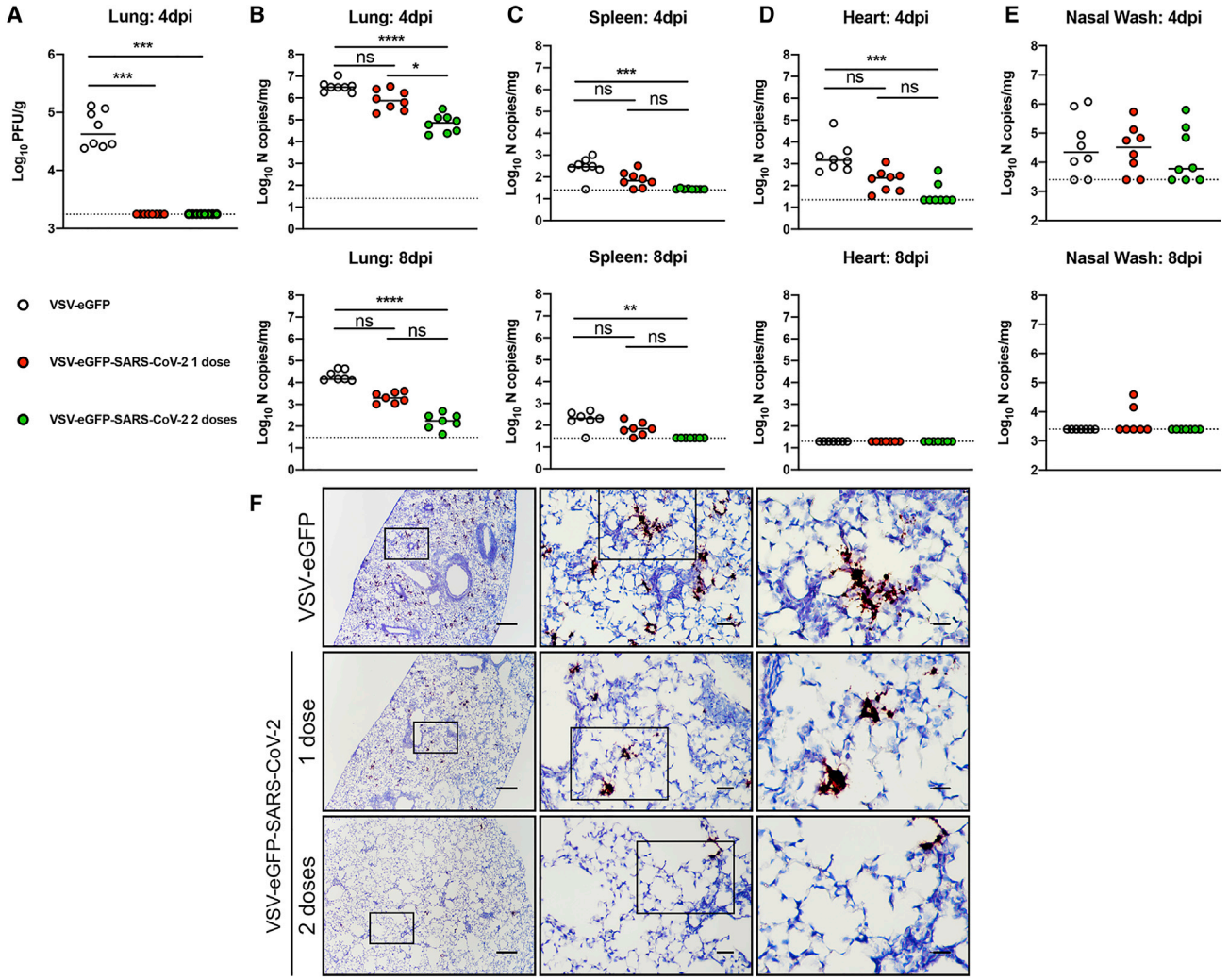

Figure 2. VSV-eGFP-SARS-CoV-2 Protects Mice against SARS-CoV-2 Infection

(A–E) Three weeks after priming or boosting with VSV-eGFP or VSV-eGFP-SARS-CoV-2, immunized animals were treated with anti-Ifnar1 mAb and one day later, animals were transduced with 2.5 × 10^8 PFU of AdV-hACE2 by intranasal administration. Five days later, animals were challenged with 3 × 10^5 PFU of SARS-CoV-2 via intranasal administration. At 4 or 8 dpi tissues were harvested, and viral burden was determined in the lung ([A] and [B]), spleen (C), heart (D), and nasal washes (E) by plaque (A) or RT-qPCR ([B]–[E]) assay (n = 7–8 mice per group; Kruskal-Wallis test with Dunn's post-test ([A]–[E]): ns, not significant, *p < 0.05, **p < 0.01, ***p < 0.001, ****p < 0.0001). Dotted lines indicate the limit of detection. Bars indicate median values.

(F) SARS-CoV-2 RNA *in situ* hybridization of lungs of mice vaccinated with VSV-eGFP or VSV-eGFP-SARS-CoV-2 and challenged with SARS-CoV-2 at 4 dpi. Images show 40×- (left; scale bars, 100 μm), 200×- (middle; scale bars, 100 μm), and 400×-magnification (right; scale bars, 10 μm; representative images from n = 3 lungs per group; 10 fields per slide).

at 8 dpi in comparison with levels seen in the control VSV-eGFP-vaccinated mice (Figures 2B–2E). The low levels of SARS-CoV-2 infection in the heart, which were observed previously in this model (Hassan et al., 2020), could be due to spread of the AdV-hACE2 from venous circulation in the lung. Mice that received two doses of VSV-eGFP-SARS-CoV-2 had significantly lower levels of viral RNA in most tissues examined compared to control VSV-eGFP vaccinated mice (Figures 2B–2E). Consistent with our viral RNA measurements, we observed less SARS-CoV-2 RNA by *in situ* hybridization in lung tissues of VSV-eGFP-SARS-CoV-2 immunized mice at 4 dpi (Figure 2F). Collectively, these data establish that immunization with VSV-eGFP-SARS-CoV-2 protects against SARS-CoV-2 infection in mice.

VSV-eGFP-SARS-CoV-2 Limits SARS-CoV-2-Induced Lung Inflammation

Both SARS-CoV and SARS-CoV-2 typically cause severe lung infection and injury that is associated with high levels of pro-inflammatory cytokines and immune cell infiltrates (Gu and Korteweg, 2007; Huang et al., 2020). The AdV-hACE2-transduced mouse model of SARS-CoV-2 pathogenesis recapitulates several aspects of lung inflammation and coronavirus disease (Hassan et al., 2020). To assess whether VSV-eGFP-SARS-CoV-2 limits virus-induced inflammation, we measured pro-inflammatory cytokine and chemokine mRNA in lung homogenates from vaccinated animals at 4 dpi by RT-qPCR assays (Figure 3A). Animals immunized with one or two doses of

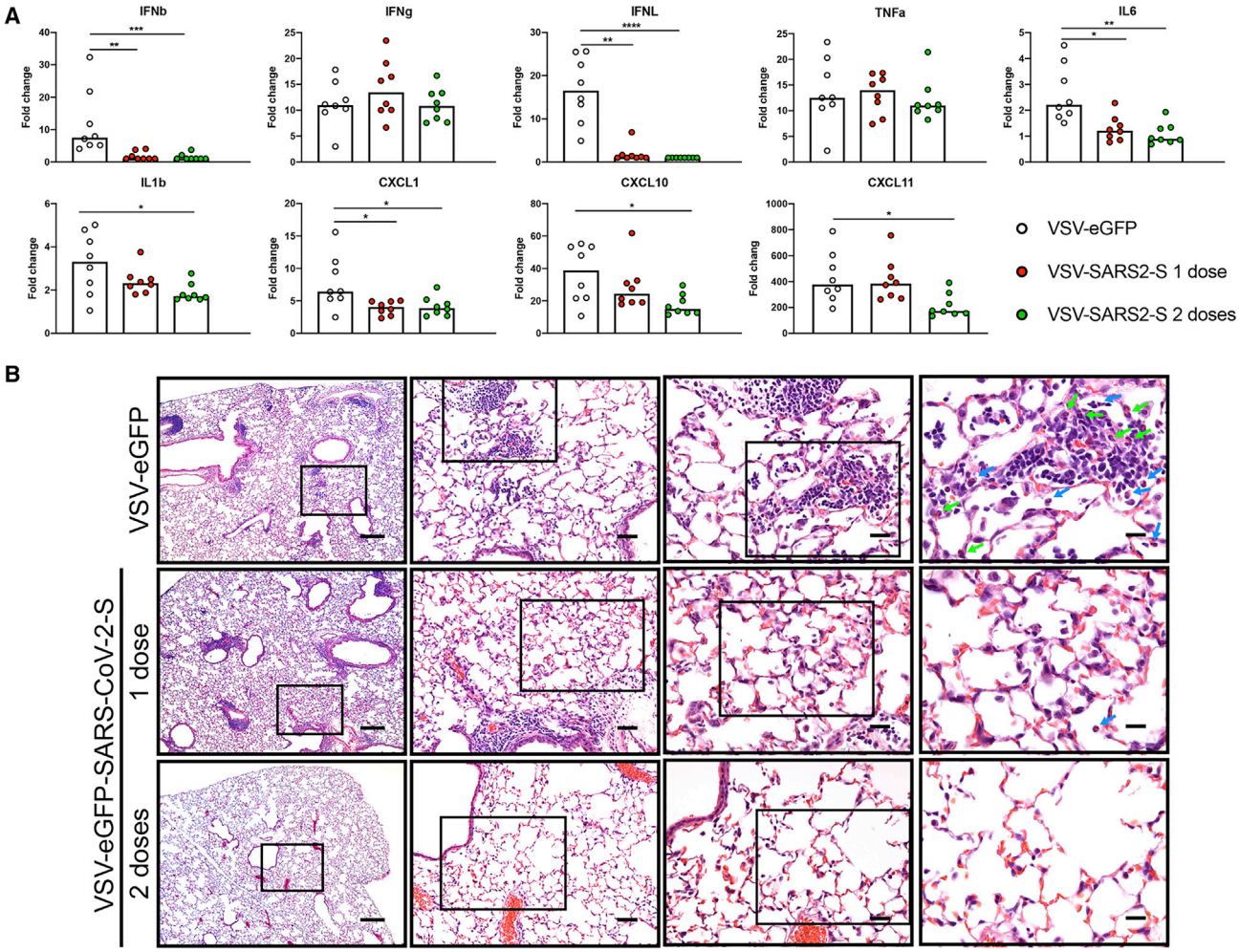

Figure 3. VSV-eGFP-SARS-CoV-2 Protects Mice from SARS-CoV-2 Lung Inflammation

(A) Lungs of VSV-eGFP- or VSV-eGFP-SARS-CoV-2-immunized mice were evaluated at 4 dpi for cytokine and chemokine expression by RT-qPCR assay. Data are shown as fold change in gene expression compared to fully naive, age-matched animals after normalization to *Gapdh* (n = 7–8 per group, Kruskal-Wallis test with Dunn's post-test: *$p < 0.05$, **$p < 0.01$, ***$p < 0.001$, ****$p < 0.0001$). Bars indicate median values.

(B) Hematoxylin and eosin staining of lung sections from immunized mice at 8 dpi with SARS-CoV-2 (3×10^5 PFU). Images show 40×- (left; scale bars, 250 μm), 200×- (second from left; scale bars, 50 μm), 400×- (third from left; scale bars, 25 μm), and 630×-magnification (right; scale bars, 10 μm). Arrows indicate neutrophils in the alveolar septum (green) and airspace (blue). Representative images are shown from n = 3 lungs per group; 10 fields per slide).

VSV-eGFP-SARS-CoV-2 had significantly lower levels of pro-inflammatory cytokine and chemokine mRNA than did VSV-eGFP vaccinated mice. Specifically, type I and III interferons (IFN-β and IFN-λ) were decreased early during infection in both one-dose and two-dose groups of mice immunized with VSV-eGFP-SARS-CoV-2. Although there were no detectable differences in IFN-γ or TNF-α levels between groups, IL-6 and IL-1β were lower at 4 dpi after VSV-eGFP-SARS-CoV-2 vaccination. Similarly, levels of mRNAs encoding chemokines CXCL1, CXCL10, and CXCL11, which recruit immune cells to the lung, were decreased at 4 dpi in VSV-eGFP-SARS-CoV-2 in comparison with VSV-eGFP immunized mice.

To determine the extent of lung pathology in SARS-CoV-2 challenged mice, at 8 dpi, we stained lung sections with hematoxylin and eosin (Figure 3B). Lung sections from VSV-eGFP-immunized mice showed immune cell (including neutrophils, arrows) infiltration into perivascular, peribronchial, and alveolar locations consistent with viral pneumonia. Lung sections from mice immunized with one dose of VSV-eGFP-SARS-CoV-2 also showed some signs of inflammation. However, mice immunized with two doses of VSV-eGFP-SARS-CoV-2 showed substantially less accumulation of inflammatory cells at the same time point after SARS-CoV-2 infection. These data suggest that immunization with VSV-eGFP-SARS-CoV-2 generates a protective immune response, which limits SARS-CoV-2-induced lung disease in mice. In this model, two sequential immunizations show greater efficacy than a single one.

Vaccine-Induced Sera Limits SARS-CoV-2 Infection

To investigate the contribution of antibodies in vaccine-mediated protection, we performed passive transfer studies. Serum was collected from VSV-eGFP and VSV-eGFP-SARS-CoV-2

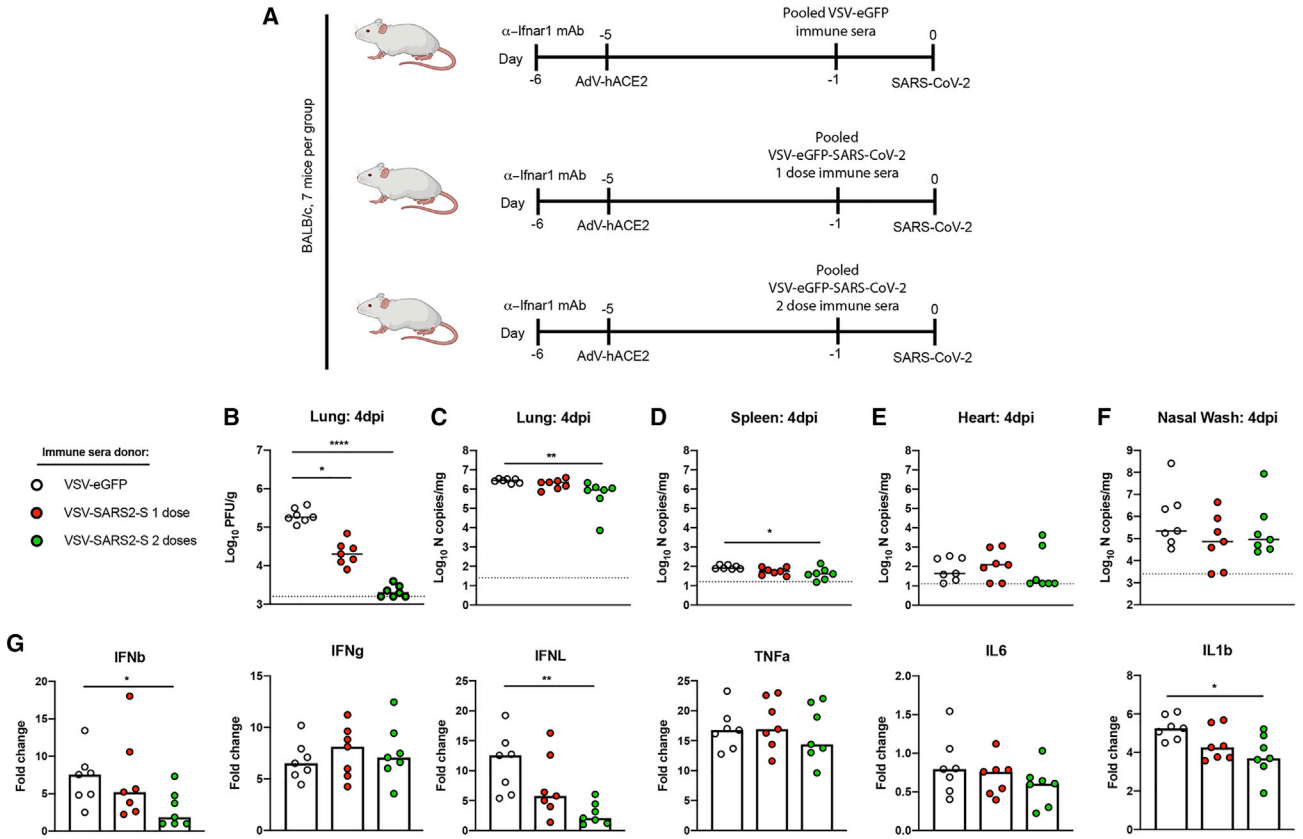

Figure 4. Vaccine-Induced Sera Limits SARS-CoV-2 Infection

(A) Passive transfer of immune sera and SARS-CoV-2 challenge scheme. Ten-week-old female BALB/c mice were treated with anti-Ifnar1 mAb, and one day later animals were transduced with 2.5 × 10^8 PFU of AdV-hACE2 by intranasal administration. Four days later, animals were administered 100 μL of pooled immune sera collected from VSV-eGFP or VSV-eGFP-SARS-CoV-2 vaccinated mice after one or two immunizations. One day later, animals were challenged with 3 × 10^5 PFU of SARS-CoV-2 via intranasal administration.

(B–F) At 4 dpi tissues were harvested, and viral burden was determined in the lung ([B] and [C]), spleen (D), heart (E), and nasal washes (F) by plaque (B) or RT-qPCR ([C]–[F]) assays (n = 7 mice per group; Kruskal-Wallis test with Dunn's post-test ([B]–[F]): *p < 0.05, **p < 0.01, ****p < 0.0001). Dotted lines indicate the limit of detection.

(G) Lungs of mice treated with immune sera were evaluated at 4 dpi for cytokine expression by RT-qPCR assay. Data are shown as fold change in gene expression compared to naive, age-matched animals after normalization to *Gapdh* (n = 7 per group, Kruskal-Wallis test with Dunn's post-test: *p < 0.05, **p < 0.01).

(B–G) Bars indicate median values.

vaccinated mice after one or two immunizations. Ten-week-old female BALB/c mice were administered anti-Ifnar1 mAb and AdV-hACE2 as described above to render animals susceptible to SARS-CoV-2. Five days later, 100 μL of pooled immune or control sera was administered by intraperitoneal injection. One day later, mice were inoculated with 3 × 10^5 PFU of SARS-CoV-2 via the intranasal route (Figure 4A). Passive transfer of sera from animals vaccinated with VSV-eGFP-SARS-CoV-2 protected against SARS-CoV-2 infection in comparison with sera from the VSV-eGFP-immunized mice. At 4 dpi, lungs from animals treated with VSV-eGFP-SARS-CoV-2 immune sera from prime-only and boosted animals showed substantially reduced infectious virus burden (Figure 4B). Although not as striking, significant decreases in viral RNA levels also were observed in the lung and spleen of animals receiving VSV-eGFP-SARS-CoV-2 boosted sera in comparison with the VSV-eGFP sera (Figures 4C and 4D). Possibly, some of the viral RNA in lung tissue homogenates after passive transfer could represent neutralized virus within cells that has not yet been cleared. Viral RNA levels in the heart of animals given sera from VSV-eGFP-SARS-CoV-2 boosted mice trended toward, but did not reach, statistical significance (Figure 4E). No effect was observed in the nasal washes of any treated group (Figure 4F), consistent with the results from our vaccinated and challenged animals (Figure 2E).

To determine the effect of the passive transfer of sera on SARS-CoV-2-mediated inflammation, we assessed the induction of several cytokines in the lung at 4 dpi (Figure 4G). Treatment with sera from animals immunized with two doses of VSV-eGFP-SARS-CoV-2 limited induction of some (IFN-β, IFN-λ, and IL-1β) pro-inflammatory cytokines after SARS-CoV-2 challenge. Together, these data suggest that antibodies are a major correlate of VSV-eGFP-SARS-CoV-2-mediated protection against SARS-CoV-2.

DISCUSSION

The emergence of SARS-CoV-2 into the human population has caused a global pandemic, resulting in millions of infected individuals and hundreds of thousands of deaths. Despite initial indications that the pandemic had peaked, reopening of countries and renewed human-to-human contact has resulted in a recent surge in case numbers, suggesting that SARS-CoV-2 vaccines will be critical for curtailing the pandemic and resuming normal social interactions. In this study, we tested the efficacy of a replication-competent VSV-eGFP-SARS-CoV-2 vaccine. A single dose of VSV-eGFP-SARS-CoV-2 was sufficient to induce antibodies in BALB/c mice that neutralize SARS-CoV-2 infection and target the RBD and S protein, and a second dose substantially boosted this response. We then challenged mice with SARS-CoV-2 via the intranasal route and observed a complete loss of recovery of infectious virus in the lung in animals immunized with either one or two doses of VSV-eGFP-SARS-CoV-2. In comparison with a single dose, administration of two doses of VSV-eGFP-SARS-CoV-2 elicited greater protection with further diminished viral loads. Immunization with VSV-eGFP-SARS-CoV-2 decreased the induction of several key pro-inflammatory cytokines and protected mice from alveolar inflammation, lung consolidation, and viral pneumonia. We also established an important role for protective antibodies, as passive transfer of immune sera from VSV-eGFP-SARS-CoV-2-immunized animals decreased viral burden and inflammation in the lung.

Recombinant VSV-based vaccines that encode viral glycoproteins have several advantages as a platform. Whereas DNA plasmid and mRNA-based vaccines have not yet been approved in the United States or elsewhere, Merck's ERVEBO, a replication-competent VSV expressing the EBOV glycoprotein, is currently in use in humans (Huttner et al., 2015). As a replicating RNA virus, VSV-based vaccines often can be used as single-dose administration and effectively stimulate both humoral and cellular immunity. Recombinant VSV grows efficiently in mammalian cell culture, enabling simple, large-scale production. Advantages of VSV as a vaccine vector also include the lack of homologous recombination and its non-segmented genome structure, which precludes genetic reassortment and enhances its safety profile (Lichty et al., 2004; Roberts et al., 1999). Other viral-based (e.g., adenoviral, Adv) vaccine vectors are limited to varying degrees (HuAdv5 > HuAdv26 > ChAdV23) by some level of preexisting immunity to the vector itself (Barouch et al., 2004; Casimiro et al., 2003; Santra et al., 2007). There is almost no preexisting human immunity to VSV, because human infections are rare (Roberts et al., 1999) with the exception of some regions of Central America (Cline, 1976) or a limited number of at-risk laboratory workers (Johnson et al., 1966).

Several vaccine candidates for SARS-CoV-2 have been tested for immunogenicity. Our VSV-eGFP-SARS-CoV-2 vaccine elicited high levels of inhibitory antibodies with median and mean serum neutralizing titers of greater than 1/5,000. Two doses of VSV-eGFP-SARS-CoV-2 induced higher neutralizing titers with more rapid onset than similar dosing of an inactivated SARS-CoV-2 vaccine in the same strain of mice (Gao et al., 2020). Consistent with these results, serum anti-S endpoint titers were higher from mice immunized with two doses of VSV-eGFP-SARS-CoV-2 (1/2,700,000) than the highest two-dose regimen of the inactivated virion vaccine (1/820,000). Two doses of DNA plasmid vaccines encoding variants of the SARS-CoV-2 S protein induced relatively modest neutralizing antibody responses (serum titer of 1/170) in rhesus macaques. Related to this, anti-S titers were approximately 1,000-fold lower after two doses of the optimal DNA vaccine (Yu et al., 2020) when compared to two doses of VSV-eGFP-SARS-CoV-2. In a pre-print study, a single-dose of a chimpanzee Adv vaccine encoding SARS-CoV-2 S protein, ChAdOx1 nCoV-19, also produced relatively low levels of serum neutralizing antibodies in mice and non-human primates (NHPs) (1/40 to 1/80 in BALB/c and CD1 mice and <1/20 in rhesus macaques). This data corresponded with anti-S1 and anti-S2 mean serum titers of between 1/100 and 1/1,000 in BALB/c mice and anti-S titers of <1/1,000 in NHPs (DOI: 10.1101/2020.05.13.093195). Two doses of a recombinant Adv5 vectored SARS-CoV-2 vaccine in humans also produced relatively low RBD binding (1/1,445 at day 28 post-boost) and neutralizing antibody (1/34 at day 28 post-boost) (Zhu et al., 2020). Finally, based on pre-print data (DOI: 10.1101/2020.06.11.145920), BALB/c mice immunized with two 1 μg doses of an mRNA vaccine candidate, mRNA-1273, elicited serum anti-S endpoint titers of 1/100,000. These mice produced mean neutralizing antibodies titers of approximately 1/1,000 and did not show evidence of infectious virus in the lung or nares after SARS-CoV-2 challenge.

Even though VSV-eGFP-SARS-CoV-2 is replication competent and capable of spread, it likely did not do so efficiently in our BALB/c mice because the SARS-CoV-2 S protein cannot efficiently utilize murine ACE2 for viral entry (Letko et al., 2020). This likely explains our need for boosting, because the response we observed likely was enabled by the residual small amount of *trans*-complementing VSV G to pseudotype the virions expressing the S protein in a manner similar to VSV-SARS (Kapadia et al., 2008), which effectively limited vaccine virus replication to a single cycle. Indeed, in transgenic animals expressing hACE2 receptors competent for S binding, a single dose of VSV-eGFP-SARS-CoV-2 was associated with greater immunogenicity, although a quantitative comparison requires more study because the backgrounds of the mice are different (H-2^d BALB/c versus H-2^b C57BL/6). Immunization and challenge studies are planned in hACE2 transgenic mice (Bao et al., 2020; Jiang et al., 2020; McCray et al., 2007; Sun et al., 2020) and in NHPs, as they become widely available. Alternatively, hamster models of SARS-CoV-2 infection have been developed with varying degrees of lung pathogenesis (Imai et al., 2020; Sia et al., 2020) and could be used to corroborate vaccine-mediated protection.

Vaccine safety is a key requirement of any platform. Pathogenicity and immunogenicity of VSV is associated with its native glycoprotein G, which, in turn, determines its pan-tropism (Martinez et al., 2003). Replacing the glycoprotein of VSV with a foreign glycoprotein often results in virus attenuation *in vivo*. Indeed, the vast majority of cases where VSV recombinants express a heterologous viral glycoprotein (e.g., chikungunya virus, H5N1 influenza virus, Lassa virus, lymphocytic choriomeningitis virus, or Ebola virus) and were injected via intracranial route into mice or NHPs, no disease was observed (Mire et al., 2012; Muik et al., 2014; van den Pol et al., 2017; Wollmann et al., 2015). One exception is when VSV expressing the glycoproteins of the highly neurotropic Nipah virus was injected via an intracranial route into

adult mice (van den Pol et al., 2017). Should substantial reactogenicity or neuronal infection be observed with VSV-eGFP-SARS-CoV-2, the vaccine could be attenuated further by introducing mutations into the matrix protein (Rabinowitz et al., 1981) or methyltransferase (Li et al., 2006; Ma et al., 2014), rearranging the order of genes (Ball et al., 1999; Wertz et al., 1998), or recoding of the L gene (Wang et al., 2015). The presence of the additional eGFP gene inserted between the leader and N genes also attenuates virus replication in cell culture (Whelan et al., 2000). Further development of a VSV vectored vaccine for SARS-CoV-2 likely will require deletion of eGFP from the genome, which could necessitate additional strategies of attenuation.

Future studies are planned to evaluate the durability of VSV-SARS-CoV-2-induced immunity. Other replication-competent VSV-based vaccines such as the rVSVΔG-ZEBOV-GP have been shown to generate long-lasting immune responses and protection (Kennedy et al., 2017). In addition, we plan to investigate in greater detail the contributions of additional arms of immunity in mediating protection. The robust induction of neutralizing antibodies elicited by one and two doses of VSV-eGFP-SARS-CoV-2 was a correlate of protection, as passive transfer of immune sera reduced viral infection and inflammation in the lung upon SARS-CoV-2 challenge. Nonetheless, it will be important to determine whether additional immune responses, particularly $CD8^+$ T cells, have an important protective role. Recently, SARS-CoV-2 specific $CD4^+$ and $CD8^+$ T cells were shown to be present in 100% and 70% of COVID-19 convalescent patients, respectively, with many of the T cells recognizing peptides derived from the S protein (Grifoni et al., 2020). Indeed, passive transfer of immune sera from vaccinated mice did not completely protect naive mice from SARS-CoV-2 infection, suggesting that T cell responses also might contribute to protection. Although VSV-eGFP-SARS-CoV-2-vaccinated mice were protected against lung infection and inflammation, nasal washes still contained high levels of SARS-CoV-2 RNA. Immunization of VSV-eGFP-SARS-CoV-2 via the intraperitoneal route, while generating systemic immunity that protects against pneumonia, likely did not generate adequate mucosal immunity to neutralize virus at the site of inoculation. This limitation potentially could be overcome by intranasal delivery of the vaccine, as described in studies with influenza A virus (Dutta et al., 2016). Finally, additional experiments are planned in aged animals (hACE2-expressing mice, hamsters, and NHPs) to address immunogenicity and protection in this key target population at greater risk for severe COVID-19. Overall, our data show that VSV-eGFP-SARS-CoV-2 can protect against severe SARS-CoV-2 infection and lung disease, supporting its further development as a vaccine.

Limitations of the Study

Our study, which used an eGFP-expressing variant of VSV-SARS-CoV-2 for tracking purposes, serves as a proof of principle for developing a replication-competent VSV vaccine platform. The next phase of studies will use VSV-SARS-CoV-2 viruses lacking the eGFP reporter gene. Another limitation that we acknowledge is that the AdV-hACE2 transduction could affect the anamnestic response in unpredictable ways because it occurs close to the time of SARS-CoV-2 challenge. Although this is a theoretical concern, we note that viral yields from organs of VSV-eGFP-control-vaccinated animals were nearly identical to those observed in SARS-CoV-2-infected unvaccinated animals (Hassan et al., 2020). More importantly, we showed robust immunogenicity of VSV-eGFP-SARS-CoV-2 in K18-hACE2 transgenic mice and that passive transfer of immune sera from VSV-eGFP-SARS-CoV-2 vaccinated to naive mice contributes to protection against SARS-CoV-2 challenge. These results indicate that humoral immunity generated by the VSV-eGFP-SARS-CoV-2 vaccine is not affected substantively by the AdV-hACE2 transduction process itself.

STAR★METHODS

Detailed methods are provided in the online version of this paper and include the following:

- KEY RESOURCES TABLE
- RESOURCE AVAILABLITY
  - Lead Contact
  - Materials Availability
  - Data and code availability
- EXPERIMENTAL MODEL AND SUBJECT DETAILS
  - Cells
  - Plasmids
  - Recombinant VSV
  - Mouse Experiments
- METHOD DETAILS
  - Gradient Purification of Recombinant Viruses
  - Measurement of Viral Burden
  - Cytokine Analysis
  - Histology and *In Situ* Hybridization
  - Neutralization Assay
  - Protein Expression and Purification
  - ELISA
- QUANTIFICATION AND STATISTICAL ANALYSIS

SUPPLEMENTAL INFORMATION

Supplemental Information can be found online at https://doi.org/10.1016/j.chom.2020.07.018.

ACKNOWLEDGMENTS

This study was supported by NIH contracts and grants (75N93019C00062, HHSN272201700060C and R01 AI127828, R37 AI059371, and U01 AI151810), the Defense Advanced Research Project Agency (HR001117S0019), NIH R01 AI130591 and R35 HL145242, the Washington University Institute of Clinical and Translational Sciences grant UL1TR002345 from the National Center for Advancing Translational Sciences (NCATS) of the National Institutes of Health (NIH), and gifts to Washington University. J.B.C. is supported by a Helen Hay Whitney Foundation postdoctoral fellowship. We thank Natalie Thornburg for providing the clinical isolate of SARS-CoV-2, Ahmed Hassan for amplifying the AdV-hACE2 stocks, James Earnest for providing cell culture support, and the Washington University School of Medicine Pulmonary Morphology Core. The content is solely the responsibility of the authors and does not necessarily represent the official view of the NIH. Some of the figures were created by using BioRender.com.

AUTHOR CONTRIBUTIONS

J.B.C. designed experiments, propagated the SARS-CoV-2 stocks, and performed VSV immunizations and SARS-CoV-2 challenge experiments. P.W.R. generated the VSV vaccines. J.B.C., R.E.C., N.M.K., J.M.F., S.S., and

CellPress

E.S.W. performed tissue harvests, histopathological studies, and viral burden analyses. B.T.M. performed *in situ* hybridization. H.Z., M.M., L.J.A., and D.H.F. designed and produced the recombinant S and RBD proteins. I.B.H. and B.K.S. performed ELISAs. S.P.K. and M.J.H. analyzed the tissue sections for histopathology. J.B.C. and R.E.C. performed neutralization assays. L.M.B. generated the VSV-eGFP control. J.B.C., P.W.R., S.P.J.W., and M.S.D. wrote the initial draft, with the other authors providing editing comments.

DECLARATION OF INTERESTS

M.S.D. is a consultant for Inbios, Vir Biotechnology, and NGM Biopharmaceuticals and is on the Scientific Advisory Board of Moderna. M.J.H. is a member of the Data and Safety Monitoring Board for AstroZeneca and founder of NuPeak Therapeutics. The Diamond laboratory has received funding under sponsored research agreements from Moderna, Vir Biotechnology, and Emergent BioSolutions. The Whelan laboratory has received funding under sponsored research agreements from Vir Biotechnology. S.P.J.W., P.W.R., M.S.D., and J.B.C. have filed a disclosure with Washington University for the recombinant VSV.

Received: July 9, 2020
Revised: July 21, 2020
Accepted: July 27, 2020
Published: July 30, 2020

REFERENCES

Alsoussi, W.B., Turner, J.S., Case, J.B., Zhao, H., Schmitz, A.J., Zhou, J.Q., Chen, R.E., Lei, T., Rizk, A.A., McIntire, K.M., et al. (2020). A Potently Neutralizing Antibody Protects Mice against SARS-CoV-2 Infection. J. Immunol. *205*, 915–922.

Amanat, F., and Krammer, F. (2020). SARS-CoV-2 Vaccines: Status Report. Immunity *52*, 583–589.

Bai, Y., Yao, L., Wei, T., Tian, F., Jin, D.Y., Chen, L., and Wang, M. (2020). Presumed Asymptomatic Carrier Transmission of COVID-19. JAMA.

Ball, L.A., Pringle, C.R., Flanagan, B., Perepelitsa, V.P., and Wertz, G.W. (1999). Phenotypic consequences of rearranging the P, M, and G genes of vesicular stomatitis virus. J. Virol. *73*, 4705–4712.

Bao, L., Deng, W., Huang, B., Gao, H., Liu, J., Ren, L., Wei, Q., Yu, P., Xu, Y., Qi, F., et al. (2020). The pathogenicity of SARS-CoV-2 in hACE2 transgenic mice. Nature *583*, 830–833.

Barouch, D.H., Pau, M.G., Custers, J.H., Koudstaal, W., Kostense, S., Havenga, M.J., Truitt, D.M., Sumida, S.M., Kishko, M.G., Arthur, J.C., et al. (2004). Immunogenicity of recombinant adenovirus serotype 35 vaccine in the presence of pre-existing anti-Ad5 immunity. J. Immunol. *172*, 6290–6297.

Baum, A., Fulton, B.O., Wloga, E., Copin, R., Pascal, K.E., Russo, V., Giordano, S., Lanza, K., Negron, N., Ni, M., et al. (2020). Antibody cocktail to SARS-CoV-2 spike protein prevents rapid mutational escape seen with individual antibodies. Science, eabd0831.

Brown, K.S., Safronetz, D., Marzi, A., Ebihara, H., and Feldmann, H. (2011). Vesicular stomatitis virus-based vaccine protects hamsters against lethal challenge with Andes virus. J. Virol. *85*, 12781–12791.

Buchholz, U.J., Finke, S., and Conzelmann, K.K. (1999). Generation of bovine respiratory syncytial virus (BRSV) from cDNA: BRSV NS2 is not essential for virus replication in tissue culture, and the human RSV leader region acts as a functional BRSV genome promoter. J. Virol. *73*, 251–259.

Case, J.B., Rothlauf, P.W., Chen, R.E., Liu, Z., Zhao, H., Kim, A.S., Bloyet, L.M., Zeng, Q., Tahan, S., Droit, L., et al. (2020). Neutralizing antibody and soluble ACE2 inhibition of a replication-competent VSV-SARS-CoV-2 and a clinical isolate of SARS-CoV-2. Cell Host Microbe, S1931-3128(20)30362-0, in press.

Casimiro, D.R., Chen, L., Fu, T.M., Evans, R.K., Caulfield, M.J., Davies, M.E., Tang, A., Chen, M., Huang, L., Harris, V., et al. (2003). Comparative immunogenicity in rhesus monkeys of DNA plasmid, recombinant vaccinia virus, and replication-defective adenovirus vectors expressing a human immunodeficiency virus type 1 gag gene. J. Virol. *77*, 6305–6313.

Chandran, K., Sullivan, N.J., Felbor, U., Whelan, S.P., and Cunningham, J.M. (2005). Endosomal proteolysis of the Ebola virus glycoprotein is necessary for infection. Science *308*, 1643–1645.

Chi, X., Yan, R., Zhang, J., Zhang, G., Zhang, Y., Hao, M., Zhang, Z., Fan, P., Dong, Y., Yang, Y., et al. (2020). A neutralizing human antibody binds to the N-terminal domain of the Spike protein of SARS-CoV-2. Science *369*, 650–655.

Cline, B.L. (1976). Ecological associations of vesicular stomatitis virus in rural Central America and Panama. Am. J. Trop. Med. Hyg. *25*, 875–883.

Dutta, A., Huang, C.T., Lin, C.Y., Chen, T.C., Lin, Y.C., Chang, C.S., and He, Y.C. (2016). Sterilizing immunity to influenza virus infection requires local antigen-specific T cell response in the lungs. Sci. Rep. *6*, 32973.

Fathi, A., Dahlke, C., and Addo, M.M. (2019). Recombinant vesicular stomatitis virus vector vaccines for WHO blueprint priority pathogens. Hum. Vaccin. Immunother. *15*, 2269–2285.

Fuerst, T.R., Niles, E.G., Studier, F.W., and Moss, B. (1986). Eukaryotic transient-expression system based on recombinant vaccinia virus that synthesizes bacteriophage T7 RNA polymerase. Proc. Natl. Acad. Sci. USA *83*, 8122–8126.

Furuyama, W., Reynolds, P., Haddock, E., Meade-White, K., Quynh Le, M., Kawaoka, Y., Feldmann, H., and Marzi, A. (2020). A single dose of a vesicular stomatitis virus-based influenza vaccine confers rapid protection against H5 viruses from different clades. NPJ Vaccines *5*, 4.

Gao, Q., Bao, L., Mao, H., Wang, L., Xu, K., Yang, M., Li, Y., Zhu, L., Wang, N., Lv, Z., et al. (2020). Rapid development of an inactivated vaccine candidate for SARS-CoV-2. Science.

Garbutt, M., Liebscher, R., Wahl-Jensen, V., Jones, S., Möller, P., Wagner, R., Volchkov, V., Klenk, H.D., Feldmann, H., and Ströher, U. (2004). Properties of replication-competent vesicular stomatitis virus vectors expressing glycoproteins of filoviruses and arenaviruses. J. Virol. *78*, 5458–5465.

Geisbert, T.W., Jones, S., Fritz, E.A., Shurtleff, A.C., Geisbert, J.B., Liebscher, R., Grolla, A., Ströher, U., Fernando, L., Daddario, K.M., et al. (2005). Development of a new vaccine for the prevention of Lassa fever. PLoS Med. *2*, e183.

Geisbert, T.W., Daddario-Dicaprio, K.M., Lewis, M.G., Geisbert, J.B., Grolla, A., Leung, A., Paragas, J., Matthias, L., Smith, M.A., Jones, S.M., et al. (2008). Vesicular stomatitis virus-based ebola vaccine is well-tolerated and protects immunocompromised nonhuman primates. PLoS Pathog. *4*, e1000225.

Grifoni, A., Weiskopf, D., Ramirez, S.I., Mateus, J., Dan, J.M., Moderbacher, C.R., Rawlings, S.A., Sutherland, A., Premkumar, L., Jadi, R.S., et al. (2020). Targets of T Cell Responses to SARS-CoV-2 Coronavirus in Humans with COVID-19 Disease and Unexposed Individuals. Cell *181*, 1489–1501.e15.

Gu, J., and Korteweg, C. (2007). Pathology and pathogenesis of severe acute respiratory syndrome. Am. J. Pathol. *170*, 1136–1147.

Hassan, A.O., Case, J.B., Winkler, E.S., Thackray, L.B., Kafai, N.M., Bailey, A.L., McCune, B.T., Fox, J.M., Chen, R.E., Alsoussi, W.B., et al. (2020). A SARS-CoV-2 Infection Model in Mice Demonstrates Protection by Neutralizing Antibodies. Cell *182*, 744–753.e4.

Henao-Restrepo, A.M., Longini, I.M., Egger, M., Dean, N.E., Edmunds, W.J., Camacho, A., Carroll, M.W., Doumbia, M., Draguez, B., Duraffour, S., et al. (2015). Efficacy and effectiveness of an rVSV-vectored vaccine expressing Ebola surface glycoprotein: interim results from the Guinea ring vaccination cluster-randomised trial. Lancet *386*, 857–866.

Henao-Restrepo, A.M., Camacho, A., Longini, I.M., Watson, C.H., Edmunds, W.J., Egger, M., Carroll, M.W., Dean, N.E., Diatta, I., Doumbia, M., et al. (2017). Efficacy and effectiveness of an rVSV-vectored vaccine in preventing Ebola virus disease: final results from the Guinea ring vaccination, open-label, cluster-randomised trial (Ebola Ça Suffit!). Lancet *389*, 505–518.

Huang, C., Wang, Y., Li, X., Ren, L., Zhao, J., Hu, Y., Zhang, L., Fan, G., Xu, J., Gu, X., et al. (2020). Clinical features of patients infected with 2019 novel coronavirus in Wuhan, China. Lancet *395*, 497–506.

Huttner, A., Dayer, J.A., Yerly, S., Combescure, C., Auderset, F., Desmeules, J., Eickmann, M., Finckh, A., Goncalves, A.R., Hooper, J.W., et al.; VSV-Ebola Consortium (2015). The effect of dose on the safety and immunogenicity of the VSV Ebola candidate vaccine: a randomised double-blind, placebo-controlled phase 1/2 trial. Lancet Infect. Dis. *15*, 1156–1166.

Imai, M., Iwatsuki-Horimoto, K., Hatta, M., Loeber, S., Halfmann, P.J., Nakajima, N., Watanabe, T., Ujie, M., Takahashi, K., Ito, M., et al. (2020). Syrian hamsters as a small animal model for SARS-CoV-2 infection and countermeasure development. Proc. Natl. Acad. Sci. USA *117*, 16587–16595.

Jia, H.P., Look, D.C., Shi, L., Hickey, M., Pewe, L., Netland, J., Farzan, M., Wohlford-Lenane, C., Perlman, S., and McCray. (2005). P.B. ACE2 receptor expression and severe acute respiratory syndrome coronavirus infection depend on differentiation of human airway epithelia. J Virol. *79*, 14614–14621.

Jiang, R.D., Liu, M.Q., Chen, Y., Shan, C., Zhou, Y.W., Shen, X.R., Li, Q., Zhang, L., Zhu, Y., Si, H.R., et al. (2020). Pathogenesis of SARS-CoV-2 in Transgenic Mice Expressing Human Angiotensin-Converting Enzyme 2. Cell *182*, 50–58.e8.

Johnson, K.M., Vogel, J.E., and Peralta, P.H. (1966). Clinical and serological response to laboratory-acquired human infection by Indiana type vesicular stomatitis virus (VSV). Am. J. Trop. Med. Hyg. *15*, 244–246.

Jones, S.M., Feldmann, H., Ströher, U., Geisbert, J.B., Fernando, L., Grolla, A., Klenk, H.D., Sullivan, N.J., Volchkov, V.E., Fritz, E.A., et al. (2005). Live attenuated recombinant vaccine protects nonhuman primates against Ebola and Marburg viruses. Nat. Med. *11*, 786–790.

Kapadia, S.U., Simon, I.D., and Rose, J.K. (2008). SARS vaccine based on a replication-defective recombinant vesicular stomatitis virus is more potent than one based on a replication-competent vector. Virology *376*, 165–172.

Kennedy, S.B., Bolay, F., Kieh, M., Grandits, G., Badio, M., Ballou, R., Eckes, R., Feinberg, M., Follmann, D., Grund, B., et al.; PREVAIL I Study Group (2017). Phase 2 Placebo-Controlled Trial of Two Vaccines to Prevent Ebola in Liberia. N. Engl. J. Med. *377*, 1438–1447.

Letko, M., Marzi, A., and Munster, V. (2020). Functional assessment of cell entry and receptor usage for SARS-CoV-2 and other lineage B betacoronaviruses. Nat. Microbiol. *5*, 562–569.

Li, J., Wang, J.T., and Whelan, S.P. (2006). A unique strategy for mRNA cap methylation used by vesicular stomatitis virus. Proc. Natl. Acad. Sci. USA *103*, 8493–8498.

Lichty, B.D., Power, A.T., Stojdl, D.F., and Bell, J.C. (2004). Vesicular stomatitis virus: re-inventing the bullet. Trends Mol. Med. *10*, 210–216.

Lurie, N., Saville, M., Hatchett, R., and Halton, J. (2020). Developing Covid-19 Vaccines at Pandemic Speed. N. Engl. J. Med. *382*, 1969–1973.

Ma, Y., Wei, Y., Zhang, X., Zhang, Y., Cai, H., Zhu, Y., Shilo, K., Oglesbee, M., Krakowka, S., Whelan, S.P., and Li, J. (2014). mRNA cap methylation influences pathogenesis of vesicular stomatitis virus in vivo. J. Virol. *88*, 2913–2926.

Martinez, I., Rodriguez, L.L., Jimenez, C., Pauszek, S.J., and Wertz, G.W. (2003). Vesicular stomatitis virus glycoprotein is a determinant of pathogenesis in swine, a natural host. J. Virol. *77*, 8039–8047.

McCray, P.B., Jr., Pewe, L., Wohlford-Lenane, C., Hickey, M., Manzel, L., Shi, L., Netland, J., Jia, H.P., Halabi, C., Sigmund, C.D., et al. (2007). Lethal infection of K18-hACE2 mice infected with severe acute respiratory syndrome coronavirus. J. Virol. *81*, 813–821.

Mire, C.E., Miller, A.D., Carville, A., Westmoreland, S.V., Geisbert, J.B., Mansfield, K.G., Feldmann, H., Hensley, L.E., and Geisbert, T.W. (2012). Recombinant vesicular stomatitis virus vaccine vectors expressing filovirus glycoproteins lack neurovirulence in nonhuman primates. PLoS Negl. Trop. Dis. *6*, e1567.

Muik, A., Stubbert, L.J., Jahedi, R.Z., Geiβ, Y., Kimpel, J., Dold, C., Tober, R., Volk, A., Klein, S., Dietrich, U., et al. (2014). Re-engineering vesicular stomatitis virus to abrogate neurotoxicity, circumvent humoral immunity, and enhance oncolytic potency. Cancer Res. *74*, 3567–3578.

Mukherjee, S., Sirohi, D., Dowd, K.A., Chen, Z., Diamond, M.S., Kuhn, R.J., and Pierson, T.C. (2016). Enhancing dengue virus maturation using a stable furin over-expressing cell line. Virology *497*, 33–40.

Pinto, D., Park, Y.J., Beltramello, M., Walls, A.C., Tortorici, M.A., Bianchi, S., Jaconi, S., Culap, K., Zatta, F., De Marco, A., et al. (2020). Cross-neutralization of SARS-CoV-2 by a human monoclonal SARS-CoV antibody. Nature *583*, 290–295.

Rabinowitz, S.G., Huprikar, J., and Dal Canto, M.C. (1981). Comparative neurovirulence of selected vesicular stomatitis virus temperature-sensitive mutants of complementation groups II and III. Infect. Immun. *33*, 120–125.

Roberts, A., Buonocore, L., Price, R., Forman, J., and Rose, J.K. (1999). Attenuated vesicular stomatitis viruses as vaccine vectors. J. Virol. *73*, 3723–3732.

Rogers, T.F., Zhao, F., Huang, D., Beutler, N., Burns, A., He, W.T., Limbo, O., Smith, C., Song, G., Woehl, J., et al. (2020). Isolation of potent SARS-CoV-2 neutralizing antibodies and protection from disease in a small animal model. Science, eabc7520.

Santra, S., Sun, Y., Parvani, J.G., Philippon, V., Wyand, M.S., Manson, K., Gomez-Yafal, A., Mazzara, G., Panicali, D., Markham, P.D., et al. (2007). Heterologous prime/boost immunization of rhesus monkeys by using diverse poxvirus vectors. J. Virol. *81*, 8563–8570.

Sheehan, K.C., Lai, K.S., Dunn, G.P., Bruce, A.T., Diamond, M.S., Heutel, J.D., Dungo-Arthur, C., Carrero, J.A., White, J.M., Hertzog, P.J., and Schreiber, R.D. (2006). Blocking monoclonal antibodies specific for mouse IFN-alpha/beta receptor subunit 1 (IFNAR-1) from mice immunized by in vivo hydrodynamic transfection. J. Interferon Cytokine Res. *26*, 804–819.

Sia, S.F., Yan, L.M., Chin, A.W.H., Fung, K., Choy, K.T., Wong, A.Y.L., Kaewpreedee, P., Perera, R.A.P.M., Poon, L.L.M., Nicholls, J.M., et al. (2020). Pathogenesis and transmission of SARS-CoV-2 in golden hamsters. Nature *583*, 834–838.

Stanifer, M.L., Cureton, D.K., and Whelan, S.P. (2011). A recombinant vesicular stomatitis virus bearing a lethal mutation in the glycoprotein gene uncovers a second site suppressor that restores fusion. J. Virol. *85*, 8105–8115.

Sun, S.H., Chen, Q., Gu, H.J., Yang, G., Wang, Y.X., Huang, X.Y., Liu, S.S., Zhang, N.N., Li, X.F., Xiong, R., et al. (2020). A Mouse Model of SARS-CoV-2 Infection and Pathogenesis. Cell Host Microbe *28*, 124–133.e4.

ter Meulen, J., van den Brink, E.N., Poon, L.L., Marissen, W.E., Leung, C.S., Cox, F., Cheung, C.Y., Bakker, A.Q., Bogaards, J.A., van Deventer, E., et al. (2006). Human monoclonal antibody combination against **SARS**coronavirus: synergy and coverage of escape mutants. PLoS Med *3*, e237, https://doi.org/10.1371/journal.pmed.0030237.

van den Pol, A.N., Mao, G., Chattopadhyay, A., Rose, J.K., and Davis, J.N. (2017). Chikungunya, Influenza, Nipah, and Semliki Forest Chimeric Viruses with Vesicular Stomatitis Virus: Actions in the Brain. J. Virol. *91*, 91.

Wang, B., Yang, C., Tekes, G., Mueller, S., Paul, A., Whelan, S.P., and Wimmer, E. (2015). Recoding of the vesicular stomatitis virus L gene by computer-aided design provides a live, attenuated vaccine candidate. MBio *6*, 6.

Wertz, G.W., Perepelitsa, V.P., and Ball, L.A. (1998). Gene rearrangement attenuates expression and lethality of a nonsegmented negative strand RNA virus. Proc. Natl. Acad. Sci. USA *95*, 3501–3506.

Whelan, S.P., Ball, L.A., Barr, J.N., and Wertz, G.T. (1995). Efficient recovery of infectious vesicular stomatitis virus entirely from cDNA clones. Proc. Natl. Acad. Sci. USA *92*, 8388–8392.

Whelan, S.P., Barr, J.N., and Wertz, G.W. (2000). Identification of a minimal size requirement for termination of vesicular stomatitis virus mRNA: implications for the mechanism of transcription. J. Virol. *74*, 8268–8276.

Wollmann, G., Drokhlyansky, E., Davis, J.N., Cepko, C., and van den Pol, A.N. (2015). Lassa-vesicular stomatitis chimeric virus safely destroys brain tumors. J. Virol. *89*, 6711–6724.

Yu, J., Tostanoski, L.H., Peter, L., Mercado, N.B., McMahan, K., Mahrokhian, S.H., Nkolola, J.P., Liu, J., Li, Z., Chandrashekar, A., et al. (2020). DNA vaccine protection against SARS-CoV-2 in rhesus macaques. Science, eabc6284.

Yuan, M., Wu, N.C., Zhu, X., Lee, C.D., So, R.T.Y., Lv, H., Mok, C.K.P., and Wilson, I.A. (2020). A highly conserved cryptic epitope in the receptor binding domains of **SARS-CoV-2** and **SARS-CoV**. Science *368*, 630–633.

Zhu, F.C., Li, Y.H., Guan, X.H., Hou, L.H., Wang, W.J., Li, J.X., Wu, S.P., Wang, B.S., Wang, Z., Wang, L., et al. (2020). Safety, tolerability, and immunogenicity of a recombinant adenovirus type-5 vectored COVID-19 vaccine: a dose-escalation, open-label, non-randomised, first-in-human trial. Lancet *395*, 1845–1854.

STAR★METHODS

KEY RESOURCES TABLE

REAGENT or RESOURCE	SOURCE	IDENTIFIER
Antibodies		
Anti-human IgG peroxidase	Sigma-Aldrich	Cat# A6029-1ML; RRID: AB_258272
CR3022	ter Meulen et al., 2006; Yuan et al., 2020	N/A
MAR1-5A3, anti-Ifnar1 mAb	Leinco	I-401; RRID: AB_2491621
Goat Anti-Mouse IgM, Human ads-HRP	SouthernBiotech	1020-05; RRID: AB_2794201
Goat Anti-Mouse IgA-HRP	SouthernBiotech	1040-05; RRID: AB_2714213
Goat Anti-Mouse IgG, Human ads-HRP	SouthernBiotech	1030-05; RRID: AB_2619742
Goat Anti-Mouse IgG1, Human ads-BIOT	SouthernBiotech	1070-08; RRID: AB_2794413
Goat Anti-Mouse IgG2b, Human ads-BIOT	SouthernBiotech	1090-08; RRID: AB_2794523
Goat Anti-Mouse IgG3, Human ads-BIOT	SouthernBiotech	1100-08; RRID: AB_2794575
Goat Anti-Mouse IgG2c, Human ads-BIOT	SouthernBiotech	1079-08; RRID: AB_2794467
Streptavidin-HRP	Invitrogen	434323; RRID: AB_2619743
Bacterial and Virus Strains		
2019 n-CoV/USA_WA1/2020	CDC (gift from Natalie Thornburg)	N/A
AdV-hACE2	Jia et al., 2005	N/A
Vaccinia virus vTF7-3	Fuerst et al., 1986	N/A
VSV-eGFP	Chandran et al., 2005	N/A
Chemicals, Peptides, and Recombinant Proteins		
Recombinant SARS-CoV-2 spike protein	Alsoussi et al.	N/A
Recombinant SARS-CoV-2 RBD protein	Alsoussi et al.	N/A
Blasticidin S HCl	GIBCO/Thermo Fisher	Cat# A1113903
Bromophenol Blue	Millipore Sigma	Cat# BX1410-7
PNGase F	New England Biolabs	Cat# P0704S
Cytosine arabinoside	Sigma-Aldrich	Cat# C1768
Formaldehyde Solution	Millipore Sigma	Cat# FX0410-5
HEPES, free acid	Millipore Sigma	Cat #5310-OP
Lipofectamine 2000 Transfection Reagent	Invitrogen/Thermo Fisher	Cat# 11668019
1-Step™ Ultra TMB-ELISA Substrate Solution	ThermoFisher Scientific	34028
TrueBlue peroxidase substrate	KPL/SeraCare	Cat# 5510-0050
Experimental Models: Cell Lines		
BSRT7/5	Buchholz et al., 1999	N/A
MA-104	ATCC	Cat# CRL-2378.1: RRID: CVCL_3846
Vero CCL81	ATCC	Cat# CCL-81: RRID: CVCL_0059
Vero E6	ATCC	Cat# CRL-1586: RRID: CVCL_0574
Vero-furin	Mukherjee et al., 2016	N/A
Experimental Models: Organisms/Strains		
Mouse: BALB/c	Jackson Laboratory	Cat#000651; RRID: IMSR_JAX:000651
Mouse: B6.Cg-Tg(K18-ACE2)2Prlmn/J	Jackson Laboratory	Cat#034860; IMSR_JAX:034860
Oligonucleotides		
SARS-CoV-2 N **F**: 5′-ATGCTGCAATCGTGCTACAA-3′	Hassan et al., 2020	N/A
SARS-CoV-2 N **R**: 5′-GACTGCCGCCTCTGCTC-3′	Hassan et al., 2020	N/A

(*Continued on next page*)

Continued

REAGENT or RESOURCE	SOURCE	IDENTIFIER
SARS-CoV-2 N **Probe**: 5′-/56-FAM/TCAAGGAAC/ ZEN/ AACATTGCCAA/3IABkFQ/-3′	Hassan et al., 2020	N/A
SARS-CoV-2 RNA ISH probe (S gene)	Advanced Cell Diagnostics	Cat# 4848561
Gapdh TaqMan Primer/Probe set	IDT	Mm.PT.39a.1
Ifng TaqMan Primer/Probe set	IDT	Mm.PT.58.41769240
Il6 TaqMan Primer/Probe set	IDT	Mm.PT.58.10005566
Il1b TaqMan Primer/Probe set	IDT	Mm.PT.58.41616450
Tnfa TaqMan Primer/Probe set	IDT	Mm.PT.58.12575861
Cxcl10 TaqMan Primer/Probe set	IDT	Mm.PT.58.43575827
Cxcl11 TaqMan Primer/Probe set	IDT	Mm.PT.58.10773148.g
Ifnb TaqMan Primer/Probe set	IDT	Mm.PT.58.30132453.g
Ifnl(2/3) TaqMan Primer/Probe set	Thermo Fisher	Mm04204156_gH
CXCL1	IDT	Mm.PT.58.42076891
Recombinant DNA		
pCAGGS-VSV-G	Stanifer et al., 2011	N/A
pGEM3-VSV L	Whelan et al., 1995	N/A
pGEM3-VSV G	Stanifer et al., 2011	N/A
pGEM3-VSV N	Whelan et al., 1995	N/A
pGEM3-VSV P	Whelan et al., 1995	N/A
pVSV-eGFP	Chandran et al., 2005	N/A
pVSV-eGFP-SARS-CoV-2-S_{AA}	Case et al., 2020	Spike mutated from MN908947.3
Software and Algorithms		
BioRender	Biorender.com	N/A
Statistics: Prism 8.0	GraphPad	N/A

RESOURCE AVAILABLITY

Lead Contact

Further information and requests for resources and reagents should be directed to and will be fulfilled by the Lead Contact, Michael S. Diamond (diamond@wusm.wustl.edu).

Materials Availability

All requests for resources and reagents should be directed to and will be fulfilled by the Lead Contact author. This includes mice, antibodies, viruses, and proteins. All reagents will be made available on request after completion of a Materials Transfer Agreement.

Data and code availability

All data supporting the findings of this study are available within the paper and are available from the corresponding author upon request.

EXPERIMENTAL MODEL AND SUBJECT DETAILS

Cells

BSRT7/5, Vero CCL81, Vero E6, Vero E6-TMPRSS2 (Case et al., 2020), and Vero-furin (Mukherjee et al., 2016) cells were maintained in humidified incubators at 34 or 37°C and 5% CO_2 in DMEM (Corning) supplemented with glucose, L-glutamine, sodium pyruvate, and 10% fetal bovine serum (FBS). MA104 cells were maintained similarly but in Medium 199 (GIBCO).

Plasmids

The S gene of SARS-CoV-2 isolate Wuhan-Hu-1 (GenBank MN908947.3) was cloned into the backbone of the infectious molecular clone of VSV containing eGFP (pVSV-eGFP) as described (Case et al., 2020). pVSV-eGFP was used as previously described, but contains a mutation K535R, the phenotype of which will be described elsewhere. Expression plasmids of VSV N, P, L, and G were previously described (Stanifer et al., 2011; Whelan et al., 1995).

Recombinant VSV

VSV-eGFP-SARS-CoV-2 and VSV-eGFP were generated and rescued as described previously (Case et al., 2020; Whelan et al., 1995). Briefly, BSRT7/5 cells (Buchholz et al., 1999) were infected with vaccinia virus encoding the bacteriophage T7 RNA polymerase (vTF7-3) (Fuerst et al., 1986) and subsequently transfected with plasmids encoding VSV N, P, L, G, and an antigenome copy of the viral genome under control of the T7 promoter. Rescue supernatants were collected 56 to 72 h post-transfection, clarified by centrifugation (5 min at 1,000 x g), and filtered through a 0.22 μm filter. Virus clones were plaque-purified on Vero CCL81 cells containing 25 μg/mL of cytosine arabinoside (Sigma-Aldrich) in the agarose overlay, and plaques were amplified on Vero CCL81 cells. All infections for generating stocks were performed at 37°C for 1 h and at 34°C thereafter. Viral supernatants were harvested upon extensive cytopathic effect and clarified of cell debris by centrifugation at 1,000 x g for 5 min. Aliquots were maintained at −80°C.

Mouse Experiments

Animal studies were carried out in accordance with the recommendations in the Guide for the Care and Use of Laboratory Animals of the National Institutes of Health. The protocols were approved by the Institutional Animal Care and Use Committee at the Washington University School of Medicine (assurance number A3381–01). Virus inoculations were performed under anesthesia that was induced and maintained with ketamine hydrochloride and xylazine, and all efforts were made to minimize animal suffering.

At four weeks of age, female BALB/c mice (Jackson Laboratory, 000651) were immunized with 10^6 PFU of VSV-eGFP-SARS-CoV-2 or VSV-eGFP in a total volume of 200 μL per mouse via the intraperitoneal route. In some immunogenicity experiments, heterozygous K18-hACE2 C57BL/6J mice (strain: 2B6.Cg-Tg(K18-ACE2)2Prlmn/J) were obtained (Jackson Laboratory, 034860) and immunized with 10^6 PFU of VSV-eGFP-SARS-CoV-2 or VSV-eGFP via an intranasal route. Where indicated, mice were boosted with homologous virus at 4 weeks post-priming. Three weeks post-priming or boosting mice were administered 2 mg of anti-Ifnar1 mAb (MAR1-5A3 (Sheehan et al., 2006), Leinco) via intraperitoneal injection. One day later, mice were administered 2.5×10^8 PFU of mouse codon-optimized AdV-hACE2 (Hassan et al., 2020) in a total volume of 50 μL per mouse via intranasal administration. Five days later, vaccinated mice were challenged with 3×10^5 PFU of SARS-CoV-2 in a total volume of 75 μL per mouse via intranasal administration. Passive transfer experiments were conducted as described above but using ten-week-old female BALB/c mice. One-hundred microliters of pooled immune sera were administered to mice in each respective group 24 h prior to SARS-CoV-2 challenge. For each immunization (prime or boost), blood from individual mice was collected twice (at days 14 and 22) from the submandibular vein. After clotting of blood at room temperature, serum was obtained and pooled.

METHOD DETAILS

Gradient Purification of Recombinant Viruses

To generate high titer stocks of VSV-eGFP, virus was grown on BSRT7/5 cells at an MOI of 3. VSV-eGFP-SARS-CoV-2 was grown on BSRT7/5 cells in the presence of VSV G, or on MA104 cells in the absence of VSV G, at MOIs of 1. To generate VSV-eGFP-SARS-CoV-2 + VSV G, BSRT7/5 cells were transfected with pCAGGS-VSV-G in Opt-MEM (GIBCO) using Lipofectamine 2000 (Invitrogen) and subsequently infected 8 to 12 h later with VSV-eGFP-SARS-CoV-2 at an MOI of 0.01 in DMEM containing 2% FBS and 20 mM HEPES pH 7.7. This VSV G decorated VSV-eGFP-SARS-CoV-2 was titrated by plaque assay and used for a larger scale infection as described above. Cell supernatants were collected after 48 h and clarified by centrifugation at 1,000 x g for 7.5 min. Supernatants were concentrated using a Beckman Optima L-100 XP ultracentrifuge (22,800 RPM x 90 min in a 70Ti fixed-angle rotor). Pellets were resuspended in 100 mM NaCl, 10 mM Tris pH 7.4, 1 mM EDTA (NTE) at 4°C overnight, and virus was banded on a 15%–45% sucrose-NTE gradient (35,000 rpm x 3 h in a SW-41Ti swinging-bucket rotor). Virus was extracted by side puncture of tubes, recovered by ultracentrifugation (22,800 RPM x 90 min in a 70Ti fixed-angle rotor) and resuspended in NTE at 4°C overnight. To determine the protein content of purified virions, samples were treated with PNGase F (New England Biolabs) according to the manufacturer's protocol to remove N-linked glycans. Samples were processed by SDS-PAGE under denaturing (100°C, 5 min) and reducing conditions (4X SDS-loading buffer containing 200 mM Tris-HCl pH 6.8, 400 mM dithiothreitol, 8% SDS, 0.4% Bromophenol Blue (Millipore Sigma), and 40% glycerol), and visualized by Coomassie staining.

Measurement of Viral Burden

Mouse tissues were weighed and homogenized with sterile zirconia beads in a MagNA Lyser instrument (Roche Life Science) in 1 mL of DMEM media supplemented to contain 2% heat-inactivated FBS. Tissue homogenates were clarified by centrifugation at 10,000 rpm for 5 min and stored at −80°C. RNA was extracted using MagMax mirVana Total RNA isolation kit (Thermo Scientific) and a Kingfisher Flex extraction machine (Thermo Scientific). Infectious viral titers in lung homogenates were determined by plaque assays on Vero-furin cells. Viral RNA levels were determined by RT-qPCR as described (Hassan et al., 2020) and normalized to tissue weight.

Cytokine Analysis

Total RNA was isolated from lung homogenates as described above and DNAase treated. cDNA was generated using the HighCapacity cDNA Reverse Transcription kit (Thermo Scientific) with the addition of RNase inhibitor according to the manufacturer's instructions. Cytokine and chemokine expression were determined using TaqMan Fast Universal PCR master mix (Thermo Scientific) with commercially available primer/probe sets specific for *IFN-γ* (IDT: Mm.PT.58.41769240), *IL-6*

(Mm.PT.58.10005566), *IL-1β* (Mm.PT.58.41616450), *TNF-α* (Mm.PT.58.12575861), *CXCL10* (Mm.PT.58.43575827), *CCL2* (Mm.PT.58.42151692), *CCL5* (Mm.PT.58.43548565), *CXCL11* (Mm.PT.58.10773148.g), *IFN-β* (Mm.PT.58.30132453.g), and *IFNλ-2/3* (Thermo Scientific Mm04204156_gH). All results were normalized to *GAPDH* (Mm.PT.39a.1) levels and the fold-change for each was determined using the $2^{-\Delta\Delta Ct}$ method comparing SARS-CoV-2 infected mice to naive controls.

Histology and *In Situ* Hybridization

Mice were euthanized, and tissues were harvested prior to lung inflation and fixation. The right lung was inflated with approximately 1.2 mL of 10% neutral buffered formalin using a 3-mL syringe and catheter inserted into the trachea. To ensure fixation of virus, inflated lungs were kept in a 40-mL suspension of neutral buffered formalin for 7 days before further processing. Tissues were paraffin-embedded and 5 μm sections were subsequently stained with hematoxylin and eosin. RNA *in situ* hybridization was performed using the RNAscope 2.5 HD Assay (Brown Kit) according to the manufacturer's instructions (Advanced Cell Diagnostics). Briefly, sections were deparaffinized and treated with H_2O_2 and Protease Plus prior to RNA probe hybridization. Probes specifically targeting SARS-CoV-2 S sequence (cat no 848561) were hybridized followed by signal amplification and detection with 3,3′-Diaminobenzidine. Tissues were counterstained with Gill's hematoxylin and an uninfected mouse was stained in parallel and used as a negative control. Pathology was evaluated from 3 lungs per group, and representative photomicrographs of 10 fields per slide were taken under investigator-blinded conditions. Tissue sections were visualized using a Nikon Eclipse microscope equipped with an Olympus DP71 color camera or a Leica DM6B microscope equipped with a Leica DFC7000T camera using 40X, 200X, or 400X magnification.

Neutralization Assay

Serial dilutions of mouse sera were incubated with 10^2 focus-forming units (FFU) of SARS-CoV-2 for 1 h at 37°C. Antibody-virus complexes were added to Vero E6 cell monolayers in 96-well plates and incubated at 37°C for 1 h. Subsequently, cells were overlaid with 1% (w/v) methylcellulose in MEM supplemented with 2% FBS. Plates were harvested 30 h later by removing overlays and fixed with 4% PFA in PBS for 20 min at room temperature. Plates were washed and sequentially incubated with 1 mg/mL of CR3022 (Yuan et al., 2020) 32245784anti-S antibody and HRP-conjugated goat anti-human IgG in PBS supplemented with 0.1% saponin and 0.1% bovine serum albumin. SARS-CoV-2-infected cell foci were visualized using TrueBlue peroxidase substrate (KPL) and quantitated on an ImmunoSpot microanalyzer (Cellular Technologies). Data were processed using Prism software (GraphPad Prism 8.0).

Protein Expression and Purification

Purified RNA from the 2019-nCoV/USA-WA1/2020 SARS-CoV-2 strain was reverse transcribed into cDNA and used as the template for recombinant gene cloning. SARS-CoV-2 RBD and S ectodomain (the S1/S2 furin cleavage site was disrupted, double proline mutations were introduced into the S2 subunit, and foldon trimerization motif was incorporated) were cloned into pFM1.2 with a C-terminal hexahistidine or octahistidine tag, transiently transfected into Expi293F cells, and purified by cobalt-charged resin chromatography (G-Biosciences) as described (Alsoussi et al., 2020).

ELISA

Six-well Maxisorp plates were coated with 2 ug/mL of either SARS-CoV-2 S or RBD protein in 50 mM Na_2CO_3 (70 μL) overnight at 4 °C. Plates were then washed with PBS + 0.05% Tween-20 and blocked with 200 μL of 1X PBS + 0.05% Tween-20 + 1% BSA + 0.02% NaN_3 for 2 h at room temperature (RT). Serum samples were serially diluted (1:3) starting at either 1:100 dilution (day 22 samples; BALB/c) or 1:100 dilution (day 21 samples; K18-hACE2) in blocking buffer. Diluted samples were added to washed plates (50 μL/well) and incubated for 1 h at RT. Bound IgG was detected using HRP-conjugated goat anti-mouse IgG (at 1:2000); bound IgM was detected using biotin-conjugated anti-mouse IgM (at 1:10000); bound IgA was detected using HRP-conjugated goat anti-mouse IgA (at 1:2000); bound IgG1 was detected using biotin-conjugated anti-mouse IgG1 (at 1:10000); bound IgG2b was detected using biotin-conjugated anti-mouse IgG2b (at 1:10000); bound IgG2c was detected using biotin-conjugated anti-mouse IgG2c (at 1:10000); and bound IgG3 was detected using biotin-conjugated anti-mouse IgG3 (at 1:10000). After washing, all plates were incubated with streptavidin-HRP (at 1:5000). Following a 1 h incubation, washed plates were developed with 50 μL of 1-Step Ultra TMB-ELISA, quenched with 2 M sulfuric acid, and the absorbance was read at 450 nm.

QUANTIFICATION AND STATISTICAL ANALYSIS

Statistical significance was assigned when *P value*s were < 0.05 using Prism Version 8.2 software (GraphPad). Tests, number of animals (n), median values, and statistical comparison groups are indicated in the Figure legends. Analysis of anti-S, anti-RBD, and neutralization titers in mice after vaccination was performed using a one-way ANOVA with Dunnett's post-test. Differences in IgG subclasses were evaluated using the Mann-Whitney test. Differences in viral titers or chemokine and cytokine levels after SARS-CoV-2 infection of immunized mice were determined using a Kruskal-Wallis test with Dunn's post-test.